Journal of ELECTRONIC MATERIALS, Vol. 45, No. 7, 2016
DOI: 10.1007/s11664-016-4505-6

Graphene Nanoplatelet–Polystyrene Nanocomposite: Dielectric and Charge Storage Behaviors

MOHAMMED H. AL-SALEH[1,3] and SAADI ABDUL JAWAD[2,4]

1.—Department of Chemical Engineering, Jordan University of Science and Technology, P.O. Box 3030, Irbid 22110, Jordan. 2.—Physics Department, Hashemite University, P.O. Box 150459, Zarqa 13115, Jordan. 3.—e-mail: mhsaleh@just.edu.jo. 4.—e-mail: saadi@hu.edu.jo

Graphene nanoplatelet (GNP)–polystyrene nanocomposites filled with up to 20 wt.% GNPs were prepared by melt mixing. The microstructure, direct-current (dc) electrical percolation behavior, and dielectric characteristics were investigated as functions of frequency. In addition, the effects of dc bias on the complex impedance and charge transport mechanisms were explored. The dc electrical percolation curve showed a gradually transition from the insulating to conducting state. At 15 wt.% GNP loading and frequency greater than 10^4 Hz, the nanocomposite exhibited dielectric constant and loss factor of 180 and 0.11, respectively, revealing remarkable storage capabilities at high frequencies. For nanocomposites filled with 12 wt.% to 20 wt.% GNPs, the alternating-current conductivity was found to follow the universal dynamic response behavior, implying electron conduction due to tunneling in addition to direct contact between GNPs.

Key words: Graphene nanoplatelets, polymer nanocomposite, dielectric properties, impedance spectroscopy, percolation behavior

INTRODUCTION

Nowadays, there is increasing interest in development of conductive and dielectric nanostructured polymeric materials based on graphene for a wide range of applications.[1–3] In polymer nanocomposites, both single- and multisheet graphene have been investigated as conductive nanofillers.[1,4–8] However, multisheet graphene, known as graphene nanoplatelets (GNPs), is more favorable because of its cost advantage over single-sheet graphene.[9,10] GNP has high aspect ratio, high electrical and thermal conductivities, and remarkable tensile properties. Moreover, GNPs are not as expensive as carbon nanotubes (CNTs), since they can be obtained by simple exfoliation of graphite. However, because of their two-dimensional (2D) geometry, GNPs are not as effective as one-dimensional (1D) CNTs in creating conductive networks in polymer matrices. Thus, GNP-based nanocomposites are expected to have higher electrical percolation threshold and lower electrical conductivity than CNT-based nanocomposites. Nonetheless, the 2D geometry of graphene is suitable for energy storage applications, and the anisotropic electrical and optical properties of graphene are considered advantageous for applications such as flexible transparent electrodes.[11] Moreover, conductive composites based on GNPs have potential applications in batteries, conductive coatings, sensors, and electromagnetic interference (EMI) shielding materials.[12]

Recently, several studies have appeared on the electrical,[13–15] dielectric,[7,16] and EMI shielding[6,8,17] characteristics of graphene–polymer nanocomposites; For example, Monti et al.[9] studied the electrical and dielectric properties of GNP–epoxy nanocomposites. The alternating-current (ac) conductivity of a nanocomposite filled with 12 wt.% GNPs was found to follow the universal dynamic response (UDR) behavior. Martin-Gallego et al.[18] compared the electrical percolation threshold (EPT) of CNT–epoxy with that of expanded graphite (EG)–epoxy. The CNT-based nanocomposite showed lower EPT because of the rod-like, 1D geometry of CNTs, which is more effective than the sheet-like, 2D

(Received November 9, 2015; accepted March 29, 2016; published online April 12, 2016)

geometry of graphene for building conductive networks. Xu et al.[19] analyzed the dielectric properties of EG–fluoroelastomer nanocomposite as functional filler loading. Nyquist plots of complex impedance were found to yield good semicircles, revealing a single relaxation time due to polarization. Paszkiewicz et al.[20] reported an EPT of only 0.05 wt.% for EG–polyethylene terephthalate prepared by *in situ* polymerization. This low percolation threshold was attributed to the high aspect ratio and perfect dispersion of the EG sheets. However, for nanocomposites prepared by dry mixing of EG powder with polymer powder, both Panwar et al.[3] and Srivastava et al.[21] reported an EPT of 2 vol.% (4 wt.%).

In this work, the microstructure, direct-current (dc) electrical properties, dielectric characteristics, and energy storage capabilities of melt-mixed GNP–polystyrene (PS) nanocomposite filled with up to 20 wt.% GNPs were investigated. In addition, the mechanisms of electron transport were investigated as a function of GNP concentration, dc bias, and frequency. Melt mixing is a favorable compounding process in the composite industry because it is simple, environmentally friendly (with no need for solvents), and cost advantageous compared with *in situ* polymerization and solution processing techniques.

EXPERIMENTAL PROCEDURES

Materials and Nanocomposite Preparation

GNP–PS nanocomposites were prepared by melt mixing in a small (55 cm^3) batch mixer (Plastograph EC, Brabender, Germany). In a typical experiment, x g GNP (xGnP-M, average diameter = 5 μm, average thickness = 7 nm, XG Sciences, USA) was mixed with 30.0 g PS (PS 125, SABIC, Saudi Arabia). The mixing conditions were as follows: mixing time 13 min (3 min for polymer fusion and 10 min for GNP–PS compounding), mixing temperature 190°C, and mixing speed 100 rpm. After melt compounding, the nanocomposites were placed in a compression molding machine (Carver Inc., USA) to prepare 1.0-mm-thick rectangular (4 cm × 2 cm) plates. The molding was conducted at 220°C and 25 MPa pressure for 10 min.

Characterization Tools

The GNP–PS microstructure was investigated by scanning electron microscopy (SEM; Quanta 450 FEG, FEI). Before imaging, the GNP–PS composites were fractured in liquid nitrogen, or thick sections of GNP–PS nanocomposite were obtained using an ultramicrotome (Reichert-Jung, Ultracut E). The thick sections and fractured surfaces were then coated with a thin layer of gold using a sputtering machine (Q150R ES, Quorum Technologies Ltd., UK). The dc electrical resistivity was measured using two setups. For nanocomposites with resistivity $>10^6$ Ω cm, a Keithley 6517B electrometer connected to a Keithley 8009 two-electrode test fixture was used. For conductive materials, a Keithley 2010 digital multimeter connected to a four-wire probe was used. The reported dc conductivities represent averages of at least four rectangular specimens.

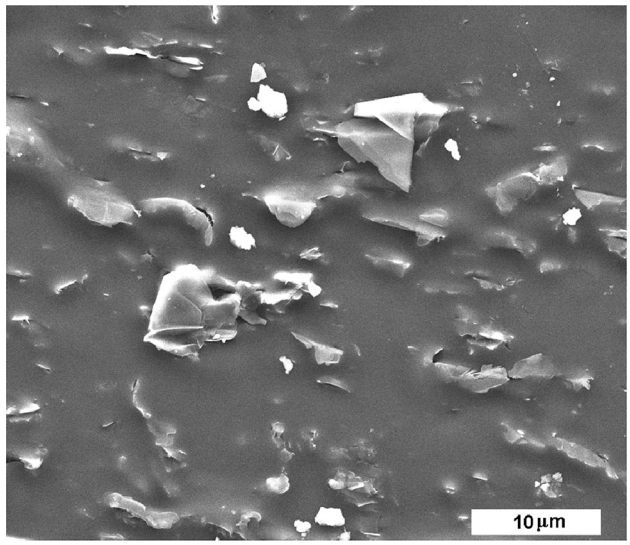

Fig. 1. SEM image of 6 wt.% GNP–PS nanocomposite.

Impedance characterization was carried out using an impedance/gain phase analyzer (Solartron-1260 with 1296 dielectric interface, Solartron Analytical). Measurements were carried out at room temperature in the dc bias range of 0 V to 4 V and frequency range of 10^0 Hz to 10^6 Hz. Z-60 and Z-View software (Scribner Associates, NC, USA) were used for data processing. Based on the obtained amplitude and phase shift of the resulting current, the components of the complex impedance components, i.e., real (Z') and imaginary (Z''), were calculated, yielding the dielectric permittivity, loss factor, and ac conductivity.

RESULTS AND DISCUSSION

Microstructure

Figure 1 shows a SEM image of the 6 wt.% GNP–PS nanocomposite. It is evident that the GNP particles are randomly dispersed within the PS matrix. These randomly dispersed particles have irregular geometry with equivalent diameter of a few microns. The absence of voids at the GNP–PS interface indicates excellent adhesion between the GNPs and PS matrix. No major agglomerates, at micron scale, were observed during SEM analysis, revealing a good level of GNP dispersion. Investigation of the GNP dispersion at nanoscale, as representatively shown in Fig. 2, showed that the GNPs were dispersed as individual sheets and aggregates of tens of GNP sheets.

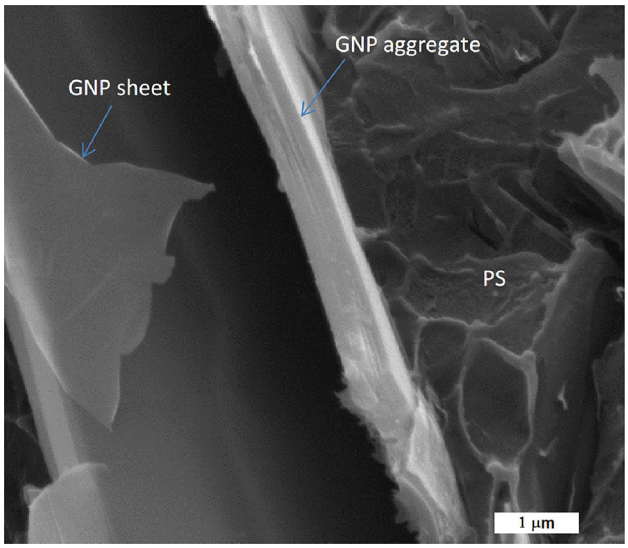

Fig. 2. High-magnification SEM image showing the dispersion of GNPs as aggregates and individual sheets.

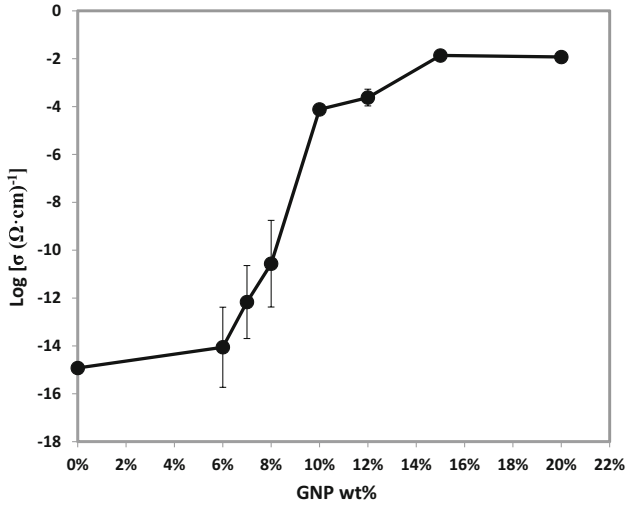

Fig. 3. Electrical percolation curve of melt-mixed GNP–PS nanocomposite.

dc Conductivity

Melt-mixed GNP–polymer nanocomposites are heterogeneous systems in which the GNP particles are randomly dispersed in the insulating PS matrix. At the EPT, the nanoparticles form a conductive network and transform the nanocomposite from the insulating to conducting state. Figure 3 shows the dc conductivity of the GNP–PS nanocomposites as a function of GNP concentration. It is apparent that, at GNP loading up to 6 wt.%, the nanocomposite is not conductive. However, in the concentration range of 7 wt.% to 10 wt.%, there is a gradual but significant increase in the electrical conductivity. In the aforementioned concentration range, the electrical conductivity increased by almost six orders of magnitude, revealing a gradual (not sharp) transformation from the insulating to conducting state. Theoretically, the EPT for the GNP–PS nanocomposite can be estimated based on the following model[22]:

$$\mathrm{EPT} = \frac{(27\pi D^2 t)}{4(D + \mathrm{IPD})^3}. \qquad (1)$$

This model was developed for nanofiller with disc-shape geometry and based on the average interparticle distance (IPD) concept.[22] In the model, D and t are the GNP diameter and thickness, respectively. For composite systems, IPD less than or equal to 10 nm is needed to allow conduction by electron tunneling.[22] Thus, based on an IPD of 10 nm and GNP dimensions of t = 7 nm and D = 5 μm (according to manufacturer information), a theoretical EPT of 3 vol.% GNPs (~6 wt.%) is obtained. However, since the GNP particles were not perfectly dispersed within the PS matrix, the experimentally obtained EPT was ~5.0 vol.% (~10 wt.%). This finding, along with the SEM microstructure analysis, reveals that the GNP dispersion is good with minor agglomerates. Further improvement in GNP dispersion would remarkably decrease the EPT.

Complex Electrical Impedance

It is widely accepted that proper analysis of dielectric relaxation profiles can provide valuable information about the microstructure and electrical properties of heterogeneous systems.[23–27] Electrical impedance is a complex quantity ($Z = Z' + iZ''$), in which the real part represents the resistance of the material while the imaginary part represents the reactance (i.e., loss factor) of the material. Based on the complex impedance, the bulk resistance and capacitance can be determined. Figure 4 depicts the real part of the complex impedance as a function of frequency and GNP concentration. For composite materials at filler loading below the electrical percolation threshold, Z' decreases with increase in frequency over the entire frequency range. This behavior was observed for composites filled with up to 10 wt.% GNPs. The inset of Fig. 4 shows the Z' profile of the 10 wt.% GNP–PS nanocomposite as an example for this behavior. However, above the EPT, the GNP–PS nanocomposites exhibited a frequency-independent plateau (resistive-like behavior) at low frequencies followed by a frequency-dependent region (capacitive-like behavior) at higher frequencies, as shown in Fig. 4 for nanocomposites filled with 12 wt.%, 15 wt.%, and 20 wt.% GNPs. Figure 4 also shows a clear decrease in the Z' plateau with increasing GNP mass fraction. This trend reflects the increase in the number of conductive pathways within the composite with increasing GNP concentration.

The frequency at which the Z' profile of the composite switches from frequency independent to frequency dependent is called the characteristic frequency (f_c). This frequency is clearly seen to increase

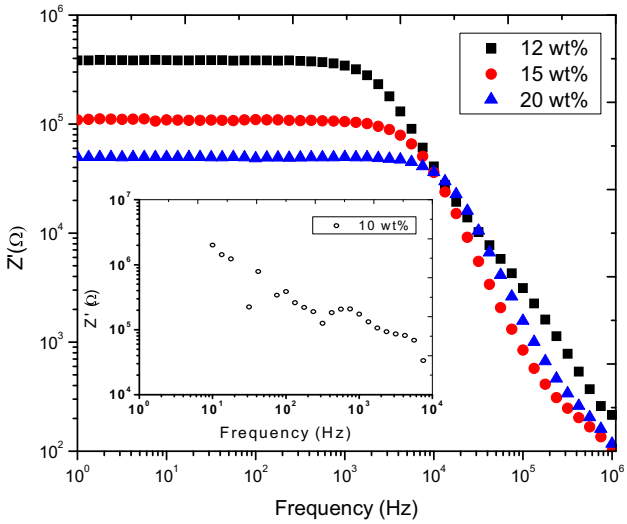

Fig. 4. Real part of complex impedance as function of frequency and GNP mass fraction. Inset shows Z' for the 10 wt.% GNP–PS nanocomposite.

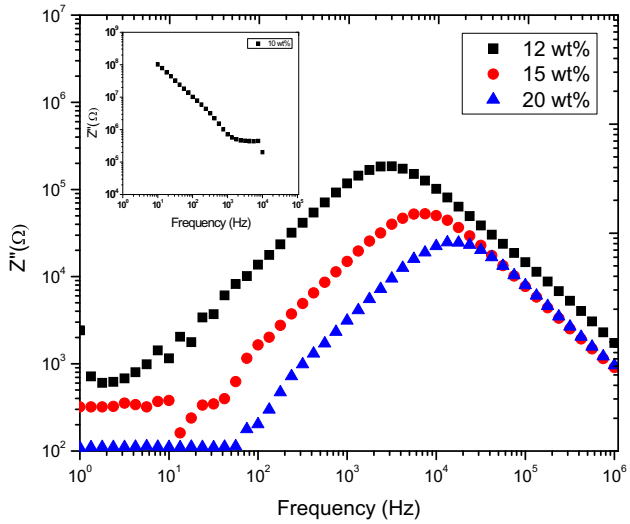

Fig. 5. Imaginary part of complex impedance as function of frequency and GNP mass fraction. Inset shows Z'' for the 10 wt.% GNP–PS nanocomposite.

with increase in the GNP content; For example, it is 4×10^2 Hz for the 12 wt.% GNP nanocomposite but 6×10^3 Hz for the 20 wt.% GNP nanocomposite. The broadening of the resistive-like region with increase in the GNP concentration can be ascribed to increase in the nanocomposite conductivity with increase in the GNP concentration.[19] However, the characteristic frequencies of the GNP–PS nanocomposites are much lower than our previously reported characteristic frequency for CNT–acrylonitrile/butadiene/styrene (ABS) nanocomposite, where an f_c of 10^4 Hz was reported for 0.25 wt.% CNT-filled nanocomposite.[28] This is related to the 1D structure of the CNTs, which is very effective for building 3D conductive networks. Nevertheless, for the 12 wt.% to 20 wt.% GNP–PS composites, the presence of both frequency-independent and frequency-dependent regions means that the conduction in this composite is due to both tunneling and direct contact between GNP particles.

The capacitive behavior of the GNP–PS nanocomposites was also confirmed from the damping profiles of Z'', as shown in Fig. 5. The GNP–PS nanocomposites showed clear damping behavior, where the peak of the imaginary impedance is seen to decrease and shift towards higher frequency with increase in the GNP concentration from 12 wt.% to 20 wt.%. This trend reflects the increase in the nanocomposite conductivity with increase in the GNP content. Similar behavior was reported for CNT–polysulfone composites[29] and exfoliated graphite–flouroelastomer composites.[19]

Nyquist Plots

Figure 6 shows Nyquist plots for the complex impedance of the GNP–PS nanocomposites. The 10 wt.% GNP–PS nanocomposite is an insulator and thus did not show semicircle behavior. However,

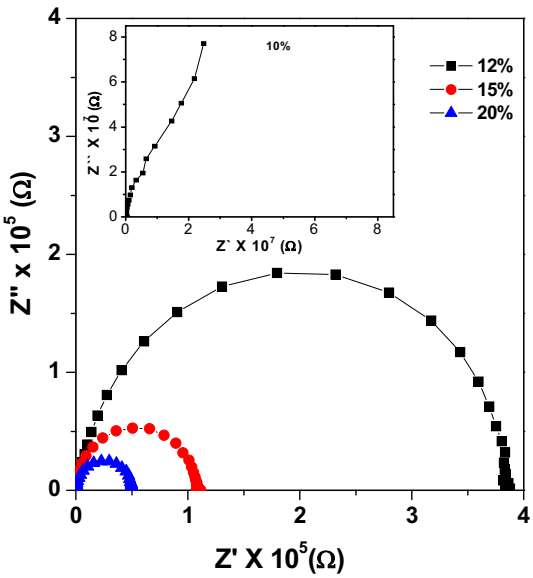

Fig. 6. Nyquist plot of GNP–PS nanocomposites. Inset shows Nyquist plot for the 10 wt.% GNP–PS nanocomposite.

the nanocomposites filled with at least 12 wt.% GNPs showed a clear semicircle, revealing the presence of a single relaxation time.[19] The diameter of the semicircle, which represents the nanocomposite resistance, decreased with increase in the GNP content. In addition, the center of the semicircle, which represents the distance between nanoparticles, is seen to move with increase in the GNP content.[30]

Permittivity

Based on the complex impedance, the complex relative permittivity ($\varepsilon = \varepsilon' + i\varepsilon''$) and loss factor [$\tan(\delta)$] can be calculated as follows:

$$\varepsilon' = \frac{Z''}{2\pi f C_0 Z^2}, \quad (2)$$

$$\varepsilon'' = \frac{Z'}{2\pi f C_0 Z^2}, \quad (3)$$

$$C_0 = \varepsilon_0 \frac{A}{d}, \quad (4)$$

$$\tan(\delta) = \frac{\varepsilon''}{\varepsilon'} = \frac{Z'}{Z''}. \quad (5)$$

In the above equations, ε' and ε'' are the real and imaginary parts of the complex relative permittivity, C_0 is the geometric capacitance, f is the frequency in Hz, ε_0 is the vacuum permittivity ($= 8.85 \times 10^{-12}$ F/m), A is the contact area between the specimen and testing electrode, and d is the thickness of the specimen. Figure 7 shows the influence of the GNP content and frequency on the permittivity. It is apparent that the dielectric constant (ε') and dielectric loss (ε'') of the nanocomposites increased with increase in the GNP concentration. The GNP particles act as capacitor electrodes,[7] the increase in concentration of which results in an increase of interfacial polarization and consequently an increase in ε' and ε''.[29,30] For the dielectric constant, it is apparent that the 15 wt.% and 20 wt.% GNP nanocomposites exhibited a constant ε' of 180 over the frequency range from 10^2 Hz to 10^6 Hz. At very low frequencies (below ~50 Hz), the dielectric constant is seen to increase significantly with decrease in frequency. This profile is related to the interfacial polarization or Maxwell–Wagner–Sillars effect.[31,32] In the low-frequency region, the remarkable decrease in ε' with no loss peak in the ε'' profile is characteristic of charged carrier systems.[31,32] Similar observations have been reported by many researchers for conductive CNT–polymer nanocomposites.[28,33]

Figure 7b shows that the dielectric loss decreases with increase in frequency and/or decrease in GNP concentration. In composite materials, ε'' reflects the contributions of dc conductance, interfacial polarization, and/or dipole orientation. The $\log(\varepsilon'')$ versus $\log(f)$ profiles show straight lines with slope of approximately -1.0 over a wide frequency region, indicating that ε'' is mainly due to dc conductance in this region.[32,34] The region of linear profile is seen to extend to higher frequencies with increase in the GNP content due to the increased GNP networks.

For energy storage applications, a material with high dielectric constant and low dissipation factor is needed.[35] In the previous section, it was found that the GNP–PS nanocomposites have remarkably high dielectric constant. To explore the potential of such nanocomposites for energy storage, the loss factor should be investigated. Figure 8 depicts the loss factor as a function of frequency. A remarkable decrease in loss factor with frequency can be

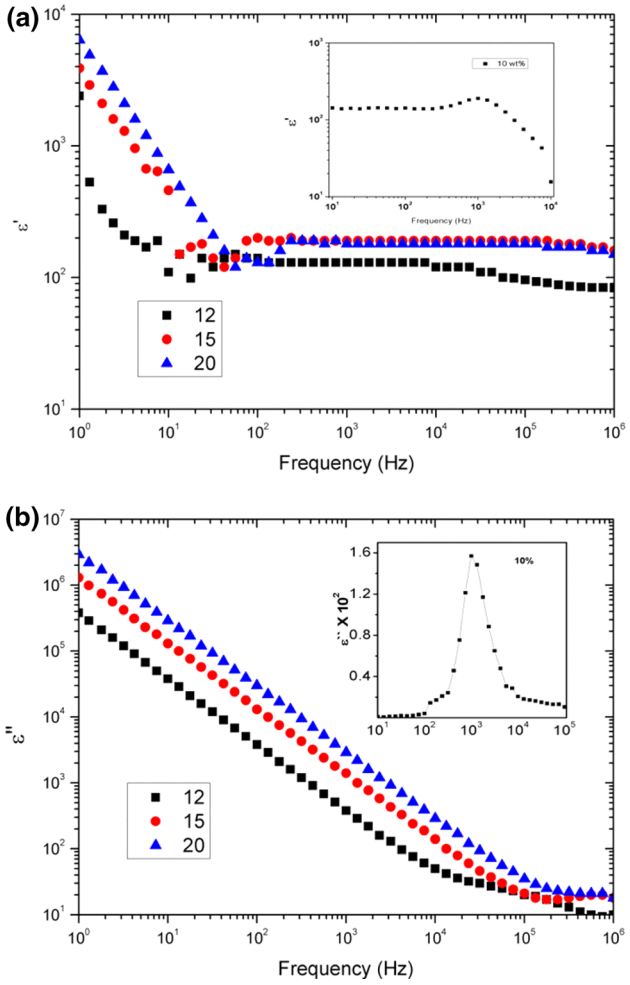

Fig. 7. Complex permittivity of GNP–PS nanocomposites as function of CNT content and frequency: (a) real and (b) imaginary part.

observed.[3] A similar observation was reported for CNT-based nanocomposite.[36] At low frequency, a loss factor as high as 700 was obtained, while at high frequencies the loss factor approached 0.12 for all nanocomposites. At high frequencies, the nanocomposite is suitable for energy storage applications, since it is characterized by dielectric constant of 180 and dissipation factor of 0.12. This value is significant compared with 1.28 wt.% CNT–polypropylene (PP), which exhibited dielectric constant of ~ 150 and loss factor of ~30.[36] Since the performance of a good dielectric depends on both the dielectric constant and the loss factor, Fig. 9 shows $\varepsilon'/\tan(\delta)$ as a function of frequency and GNP content. It is apparent that the GNP–PS nanocomposites exhibit poor energy storage capabilities at low frequencies. However, at high frequencies, $\varepsilon'/\tan(\delta)$ values exceeding 1000 can be obtained. This value exceeds the recently reported $\varepsilon'/\tan(\delta)$ values for foamed CNT–PP nanocomposite [$\varepsilon'/\tan(\delta) = 500$], graphene oxide–polyurethane nanocomposite [$\varepsilon'/\tan(\delta) = 500$], and polypyrrole-modified CNT–PS nanocomposite [$\varepsilon'/\tan(\delta) = 630$].[37] However, the GNP–PS nanocomposite suffers from instability of

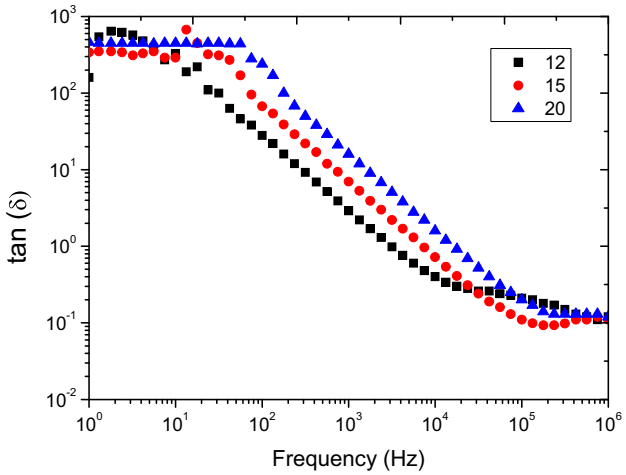

Fig. 8. Dissipation factor as function of frequency of GNP–PS nanocomposites.

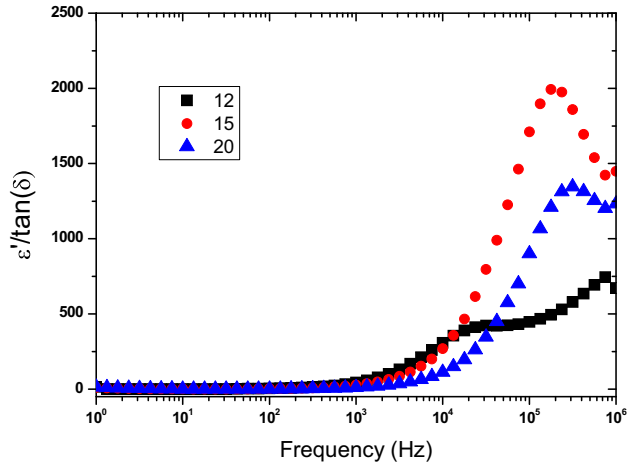

Fig. 9. Performance of GNP–PS nanocomposites as function of frequency and GNP content.

tan(δ) with frequency, thus more work is needed to enhance the stability of the loss factor over a wide range of frequencies.

ac Conductivity

The ac conductivity (σ_{ac}) behavior has been widely used to probe the conduction mechanisms of polymer nanocomposites.[38] The ac conductivity can be calculated as follows:

$$\sigma_{ac} = 2\pi f \varepsilon_0 \varepsilon''. \quad (6)$$

Figure 10 shows the effects of the GNP concentration and frequency on σ_{ac} of the GNP–PS nanocomposites. It is evident that the log(σ_{ac}) versus log(f) profiles can be divided into two distinct zones following the UDR model, expressed as[39]:

$$\sigma_{ac} = \sigma' + A\omega^s. \quad (7)$$

In the UDR model, σ' is the plateau of σ_{ac} (i.e., the frequency-independent conductivity), A and s are constants, and ω is the angular frequency. In ac characterization, σ' is typically called σ_{dc}; however, herein and in order to eliminate any confusion between the dc conductivity measured by the dc setup and the plateau of the σ_{ac} spectra, the plateau of the σ_{ac} spectra is called σ'. According to Fig. 10, the ac conductivity profiles of the GNP–PS nanocomposites consist of two parts. The first part is frequency independent and reflects the conductivity due to direct contact between GNP particles, while the second part is frequency dependent ($A\omega^s$) and reflects the conductivity due to tunneling and hopping of electrons between adjacent particles. This behavior has been reported for nanocomposites based on CNTs,[28,29,40] carbon black,[30] copper nanowires,[41] and EG.[18,19] It is apparent that, with increase in the GNP concentration (i.e., increase in conductive networks), σ' increased and the frequency-independent

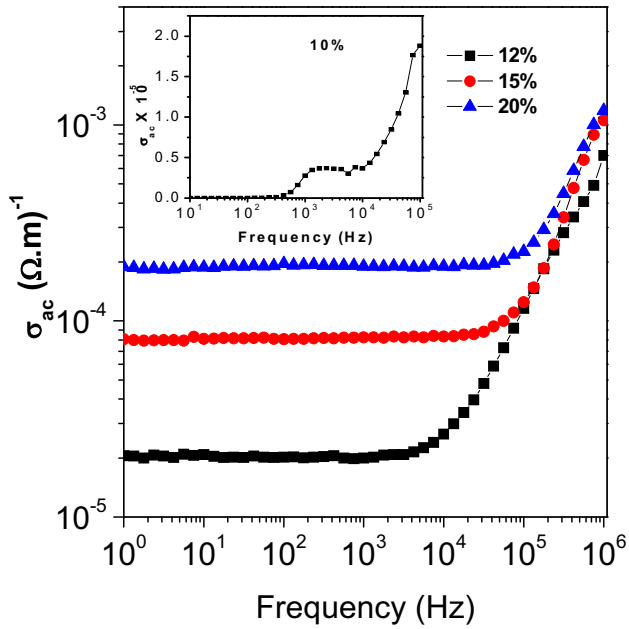

Fig. 10. ac conductivity of GNP–PS nanocomposites as function of frequency and GNP content.

region broadened to higher frequencies. In the frequency-dependent region, the increase in conductivity with frequency can be attributed to removal of any charge buildup due to space charge.

Effect of dc Bias

The effects of dc bias on the dielectric properties of 12 wt.%, 15 wt.%, and 20 wt.% GNP–PS nanocomposites were investigated. Identical responses were obtained regardless of the nanofiller content. Thus, in this section, we show only profiles for the 15 wt.% GNP–PS nanocomposite. Figure 11 shows Z' and Z'' for the 15 wt.% GNP–PS nanocomposite as functions of frequency and dc bias. Two major zones can be

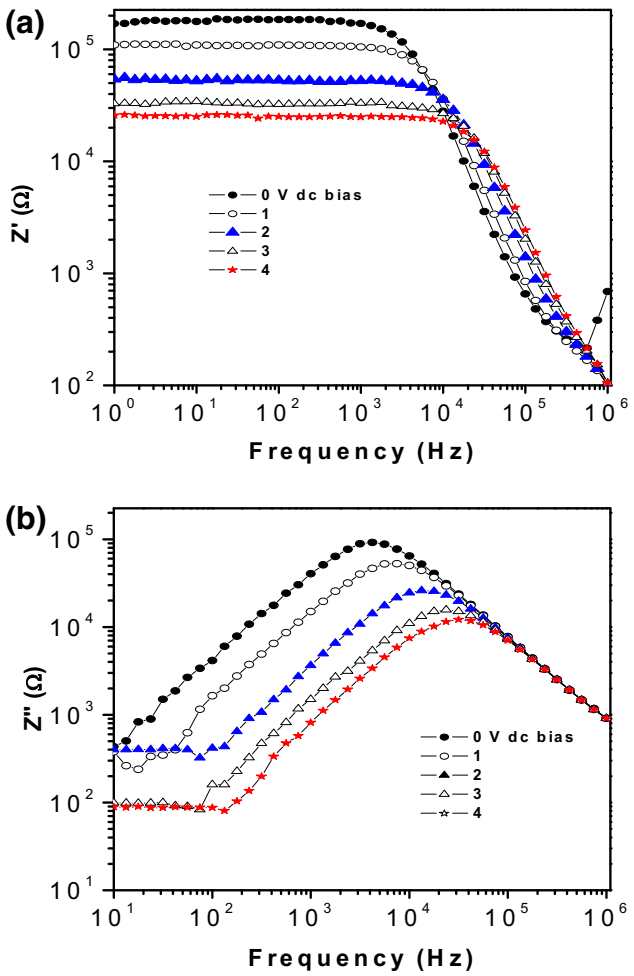

Fig. 11. Effect of dc bias on impedance Z' (a) and Z'' (b) of 15 wt.% GNP–PS nanocomposite.

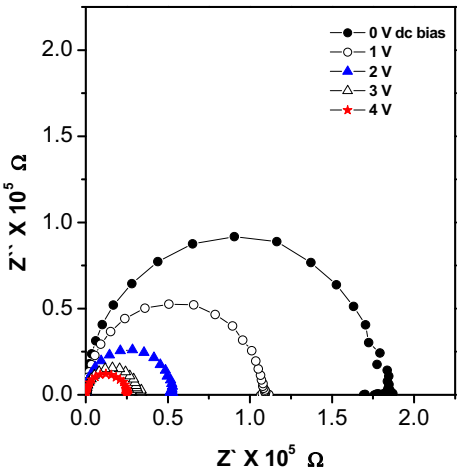

Fig. 12. Nyquist plot of 15 wt.% GNP–PS nanocomposite as function of dc bias.

observed in the Z' versus log(f) profile. The first zone is the frequency-independent zone, which is seen to broaden with increase in the dc bias. The presence of

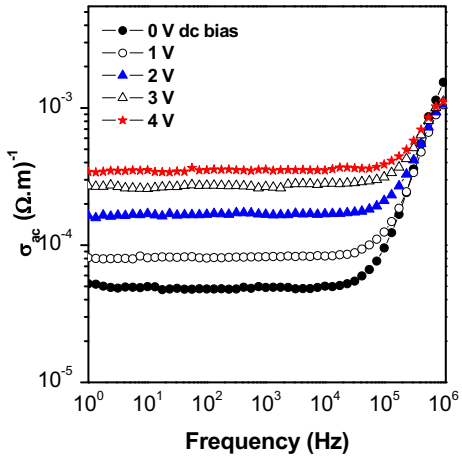

Fig. 13. Influence of dc bias on conductivity of 15 wt.% GNP–PS nanocomposite.

this zone over a wide range of dc bias indicates that direct contact between particles is the dominant conduction mechanism. The second clear zone is the frequency-dependent zone, in which Z' remarkably decreases with frequency. Also, in this high-frequency region, Z'' exhibited a well-defined relaxation peak and Nyquist plots of the complex impedance showed semicircles, as shown in Fig. 12. The diameter of the semicircles is clearly seen to decrease with increase in the dc bias. Figure 13 depicts the influence of the dc bias on the ac conductivity as a function of frequency. It is apparent that the ac conductivity follows the UDR behavior. In addition, the critical frequency at which the ac conductivity transforms from frequency independent to frequency dependent increases with increase in the dc bias due to the increase in electron tunneling between adjacent particles.

CONCLUSIONS

GNP–PS nanocomposites filled with up to 20 wt.% GNPs were prepared by melt mixing. The microstructure, electrical percolation behavior, and dielectric properties of the nanocomposites were investigated to reveal the conduction mechanisms as a function of GNP content and dc bias. In addition, the energy storage capabilities of the nanocomposites were investigated. The nanocomposites exhibited a good level of GNP dispersion with electrical percolation threshold of ~10 wt.%. The dc conductivity, ac conductivity plateau, and characteristic frequency were found to increase with increase in the GNP content, because of the construction of more GNP networks. For nanocomposites filled with 12 wt.% to 20 wt.% GNPs, two distinct zones according to the UDR model were observed in ac conductivity versus frequency plots. The presence of both frequency-dependent and frequency-independent zones means that conduction in these nanocomposites is due to tunneling and direct contact between GNP particles. At

frequency above 10^4 Hz, the 15 wt.% GNP–PS nanocomposite exhibited remarkable storage capabilities with dielectric constant and loss factor of 180 and 0.11, respectively.

REFERENCES

1. A. Nasir, A. Kausar, and A. Younus, *Polym. Plast. Technol. Eng.* 54, 750 (2015).
2. J. Du and H.-M. Cheng, *Macromol. Chem. Phys.* 213, 1060 (2012).
3. V. Panwar, B. Kang, J.-O. Park, S. Park, and R.M. Mehra, *Eur. Polym. J.* 45, 1777 (2009).
4. D.-X. Yan, H. Pang, B. Li, R. Vajtai, L. Xu, P.-G. Ren, J.-H. Wang, and Z.-M. Li, *Adv. Funct. Mater.* 25, 559 (2015).
5. A.P. Singh, M. Mishra, D.P. Hashim, T.N. Narayanan, M.G. Hahm, P. Kumar, J. Dwivedi, G. Kedawat, A. Gupta, B.P. Singh, A. Chandra, R. Vajtai, S.K. Dhawan, P.M. Ajayan, and B.K. Gupta, *Carbon* 85, 79 (2015).
6. Y. Chen, Y. Wang, H.-B. Zhang, X. Li, C.-X. Gui, and Z.-Z. Yu, *Carbon* 82, 67 (2015).
7. N. Yousefi, X. Sun, X. Lin, X. Shen, J. Jia, B. Zhang, B. Tang, M. Chan, and J.-K. Kim, *Adv. Mater.* 26, 5480 (2014).
8. R.R. Mohan, S.J. Varma, M. Faisal, and S. Jeyalekshmi, *RSC Adv.* 5, 5917 (2014).
9. M. Monti, M. Rallini, D. Puglia, L. Peponi, L. Torre, and J.M. Kenny, *Compos. Part Appl. Sci. Manuf.* 46, 166 (2013).
10. E.V. Kuvardina, L.A. Novokshonova, S.M. Lomakin, S.A. Timan, and I.A. Tchmutin, *J. Appl. Polym. Sci.* 128, 1417 (2013).
11. Y.T. Liang and M.C. Hersam, *J. Am. Chem. Soc.* 132, 17661 (2010).
12. D. Ponnamma and K.K. Sadasivuni, *Graphene-Based Polymer Nanocomposites Electrons*, ed. K.K. Sadasivuni, D. Ponnamma, J. Kim, and S. Thomas (New York: Springer, 2015), pp. 1–24.
13. J.A. King, D.R. Klimek, I. Miskioglu, and G.M. Odegard, *J. Appl. Polym. Sci.* 128, 4217 (2013).
14. F.D.C. Fim, N.R.S. Basso, A.P. Graebin, D.S. Azambuja, and G.B. Galland, *J. Appl. Polym. Sci.* 128, 2630 (2013).
15. İ. Mutlay and L.B. Tudoran, *Fuller. Nanotub. Carbon Nanostruct.* 22, 413 (2014).
16. Y. Wu, X. Lin, X. Shen, X. Sun, X. Liu, Z. Wang, and J.-K. Kim, *Carbon* 89, 102 (2015).
17. J. Liang, Y. Wang, Y. Huang, Y. Ma, Z. Liu, J. Cai, C. Zhang, H. Gao, and Y. Chen, *Carbon* 47, 922 (2009).
18. M. Martin-Gallego, M. Hernández, V. Lorenzo, R. Verdejo, M.A. Lopez-Manchado, and M. Sangermano, *Polymer* 53, 1831 (2012).
19. D. Xu, V. Sridhar, S.P. Mahapatra, and J.K. Kim, *J. Appl. Polym. Sci.* 111, 1358 (2009).
20. S. Paszkiewicz, A. Szymczyk, Z. Špitalský, M. Soccio, J. Mosnáček, T.A. Ezquerra, and Z. Rosłaniec, *J. Polym. Sci. Part B Polym. Phys.* 50, 1645 (2012).
21. N.K. Srivastava and R.M. Mehra, *Mater. Sci. Pol.* 27, 109 (2009).
22. J. Li and J.-K. Kim, *Compos. Sci. Technol.* 67, 2114 (2007).
23. K. Asami, *Prog. Polym. Sci.* 27, 1617 (2002).
24. B.K. Money, K. Hariharan, and J. Swenson, *Solid State Ion.* 225, 346 (2012).
25. S.P. Mahapatra, D.K. Tripathy, and Y. Lee, *Polym. Bull.* 68, 1965 (2012).
26. S. Choudhary and R.J. Sengwa, *J. Appl. Polym. Sci.* 124, 4847 (2012).
27. S. Choudhary and R.J. Sengwa, *Ionics* 17, 811 (2011).
28. M.H. Al-Saleh, H.K. Al-Anid, Y.A. Husain, H.M. El-Ghanem, and S.A. Jawad, *J. Phys. Appl. Phys.* 46, 385305 (2013).
29. L. Nayak, D. Khastgir, and T.K. Chaki, *Polym. Compos.* 33, 85 (2012).
30. B. Sahoo, K. Naskar, K. Dubey, R. Choudhary, and D. Tripathy, *J. Mater. Sci.* 48, 702 (2013).
31. B.G. Soares, M.E. Leyva, G.M.O. Barra, and D. Khastgir, *Eur. Polym. J.* 42, 676 (2006).
32. Y. Xi, Y. Bin, C.K. Chiang, and M. Matsuo, *Carbon* 45, 1302 (2007).
33. A. Ameli, S. Wang, Y. Kazemi, C.B. Park, and P. Pötschke, *Nano Energy* 15, 54 (2015).
34. S. Abdul Jawad, A.S. Abu-Surrah, M. Maghrabi, and Z. Khattari, *Phys. B Condens. Matter* 406, 2565 (2011).
35. R.R. Kohlmeyer, A. Javadi, B. Pradhan, S. Pilla, K. Setyowati, J. Chen, and S. Gong, *J. Phys. Chem. C* 113, 17626 (2009).
36. A. Ameli, M. Nofar, C.B. Park, P. Pötschke, and G. Rizvi, *Carbon* 71, 206 (2014).
37. C. Yang, Y. Lin, and C.W. Nan, *Carbon* 47, 1096 (2009).
38. C.S. Suchand Sangeeth, R. Kannan, V.K. Pillai, and R. Menon, *J. Appl. Phys.* 112, 053706 (2012).
39. A.K. Jonscher, *Nature* 267, 673 (1977).
40. A. Vavouliotis, E. Fiamegou, P. Karapappas, G.C. Psarras, and V. Kostopoulos, *Polym. Compos.* 31, 1874 (2010).
41. A.B. da Silva, M. Arjmand, U. Sundararaj, and R.E.S. Bretas, *Polymer* 55, 226 (2014).